INTERNATIONAL JOURNAL FOR NUMERICAL METHODS IN FLUIDS
*Int. J. Numer. Meth. Fluids* **30**: 461–479 (1999)

# TWO-DIMENSIONAL SHALLOW WATER EQUATIONS BY COMPOSITE SCHEMES

RICHARD LISKA[a,*,1] AND BURTON WENDROFF[b,2]

[a] *Faculty of Nuclear Sciences and Physical Engineering, Czech Technical University in Prague, Břehová 7, 115 19 Prague 1, Czech Republic*
[b] *Group T-7, Los Alamos National Laboratory, Los Alamos, NM 87544, USA*

## SUMMARY

Composite schemes are formed by global composition of several Lax–Wendroff steps followed by a diffusive Lax–Friedrichs or WENO step, which filters out the oscillations around shocks typical for the Lax–Wendroff scheme. These schemes are applied to the shallow water equations in two dimensions. The Lax–Friedrichs composite is also formulated for a trapezoidal mesh, which is necessary in several example problems. The suitability of the composite schemes for the shallow water equations is demonstrated on several examples, including the circular dam break problem, the shock focusing problem and supercritical channel flow problems. Copyright © 1999 John Wiley & Sons, Ltd.

KEY WORDS: shallow water equations; composite schemes; conservation laws; Lax–Friedrichs scheme; Lax–Wendroff scheme

## 1. INTRODUCTION

The shallow water equations are a system of conservation laws. There are two simple well-known finite difference schemes for conservation laws, Lax–Wendroff (LW) and Lax–Friedrichs (LF). Both of these methods have some drawbacks. The LW scheme is second-order-accurate but oscillatory close to shocks. The LF scheme is non-oscillatory but also excessively diffusive. Composite schemes combine these two methods in an attempt to remove their deficiencies. One example of a composite scheme is a global composition of several LW steps followed by one diffusive LF step that serves as a consistent filter removing the unwanted oscillations. This simple construction is efficient and produces surprisingly good results. For more details see [1]. Another composite uses a component-wise formulation of WENO for the diffusive step. Here, the authors apply these composite schemes to the shallow water equations in two dimensions.

* Correspondence to: Faculty of Nuclear Sciences and Physical Engineering, Czech Technical University in Prague, Břehová 7, 115 19 Prague 1, Czech Republic. Tel.: +420 2 21912272; fax: +420 2 6884818; e-mail: liska@siduri.fjfi.cvut.cz
[1] http://www-troja.fjfi.cvut.cz/~liska
[2] E-mail: bbw@lanl.gov, http://math.unm.edu/~bbw

Contract/grant sponsor: The CHAMMP Program
Contract/grant sponsor: National Science Foundation; Contract/grant number: CCR-9531828
Contract/grant sponsor: Czech Ministry of Education; Contract/grant number: Kontakt ME 050 (1997)

CCC 0271–2091/99/120461–19$17.50

*Received March 1998*
*Revised July 1998*

The two-dimensional shallow water equations have attracted quite a lot of attention in recent years. Alcrudo and Garcia-Navarro [2] developed a high-resolution Godunov-type MUSCL finite volume scheme. Glaister [3] used a flux splitting technique. Nadiga [4] designed an adaptive discrete velocity model of the shallow water equations. Nadiga *et al.* [5] employed a semi-Lagrangian scheme on a massively parallel computer. Zienkiewicz and Ortiz [6] introduced a split characteristic finite element method. Ambrosi [7] used Roe's Riemann solver with MUSCL slope limiting. Bova and Carey [8] developed a streamline upwind Petrov–Galerkin scheme. Morel *et al.* [9] decomposed the shallow water equations into many advection equations, which are then solved by a finite volume scheme with a special limiter. Lyra and Morgan [10] used Galerkin–LED and MUSCL schemes on an adaptive unstructured mesh. More recently, in 1997, Walters and Barragy [11] compared $H$ and $P$ finite element methods. Anastasiou and Chan [12] used a Godunov-type second-order upwind finite volume method on unstructured triangular meshes. Chippada *et al.* [13] developed a Godunov-type finite volume method using Roe's approximation for solving the Riemann problems. Apparently, there are many numerical methods for solving the shallow water equations. This paper applies composite schemes to solve this problem and show that they work remarkably well.

The paper is organized as follows. Section 2 illustrates how composite schemes work for the shallow water equations in one dimension. Section 3 presents the shallow water equations in two dimensions and the boundary conditions used. Section 4 covers the finite difference schemes on uniform rectangular meshes. In Section 5, the finite difference schemes are newly developed on trapezoidal meshes, which are needed for channel flow problems. Section 6 includes several numerical test problems demonstrating the usefulness of the composite schemes for the shallow water equations.

## 2. ONE-DIMENSIONAL ILLUSTRATION

The shallow water equations [14] in one dimension are

$$h_t + (hu)_x = 0,$$

$$(hu)_t + \left( hu^2 + g\frac{1}{2}h^2 \right)_x + ghz_{0x} = 0.$$

Here $h(x, t)$ is the thickness of the water layer, $u(x, t)$ is the velocity of the layer, $z_0(x)$ is the height of the bottom profile and $g$ is the gravitational constant. The authors use here the bottom profile

$$z_0(x) = \begin{cases} b_c\left(1 - \dfrac{x^2}{4}\right) & \text{for } -2 \le x \le 2 \\ 0 & \text{otherwise.} \end{cases}$$

The initial conditions $h(x, 0) + z_0(x) = 1$, $u(x, 0) = u_0$ set the height of the water surface and the initial velocity to be constant. Free boundary conditions are applied.

For a system of conservation laws

$$U_t = f_x(U),$$

 

the two-step Lax–Friedrichs (LF) scheme defines new values on a staggered dual grid as

$$U_{i+1/2}^{n+1/2} = \frac{1}{2}[U_i^n + U_{i+1}^n] + \frac{\Delta t}{2\Delta x}[f(U_{i+1}^n) - f(U_i^n)], \tag{1}$$

and the solution on the original grid is obtained by the same formula shifted by 1/2 in the index $i$. The two-step Lax–Wendroff (LW) scheme uses the same predictor (1) for the first half-step. In the second half-step, however, it advances from the time level $n$ to the time level $n+1$ using the fluxes from the time level $n+1/2$,

$$U_i^{n+1} = U_i^n + \frac{\Delta t}{\Delta x}[f(U_{i+1/2}^{n+1/2}) - f(U_{i-1/2}^{n+1/2})]. \tag{2}$$

It is well-known that the LW scheme produces oscillations behind shocks, while LF is excessively diffusive, smearing out the shocks. Both these phenomena are evident in Figure 1, where the heights at $t = 20$ of the one-dimensional shallow water flow over topography calculated by LF and LW schemes with 250 points is presented. In this problem, the authors used $b_c = 0.2$, $u_0 = 1$, $g = 1$ and solved it in $x \in (-10, 10)$.

The composite scheme is defined by global composition of several LW steps followed by one LF step. The operator defined by the LW scheme (1) and (2) is denoted $L_W$, and the operator defined by the LF scheme (1) by $L_F$, with both operators doing one time step from time level $n$ to $n+1$. The difference operator $S_k$ defined by $k-1$ applications of $L_W$ followed by one application of $L_F$

$$S_k = L_F \circ L_W \circ \cdots \circ L_W, \tag{3}$$

then defines the composite scheme, which is called LWLF$k$. The operator $S_k$ operates from time level $n$ to $n+k$, $U^{n+k} = S_k U^n$. The results of the same problem done by the composite LWLF4 scheme with 250 and 2000 points presented in Figure 2 shows that the composite scheme eliminates the drawbacks of both LW and LF schemes. The solution is not oscillatory and the shock heights and speeds are resolved well. The solution with 2000 points should be a good approximation of the exact solution.

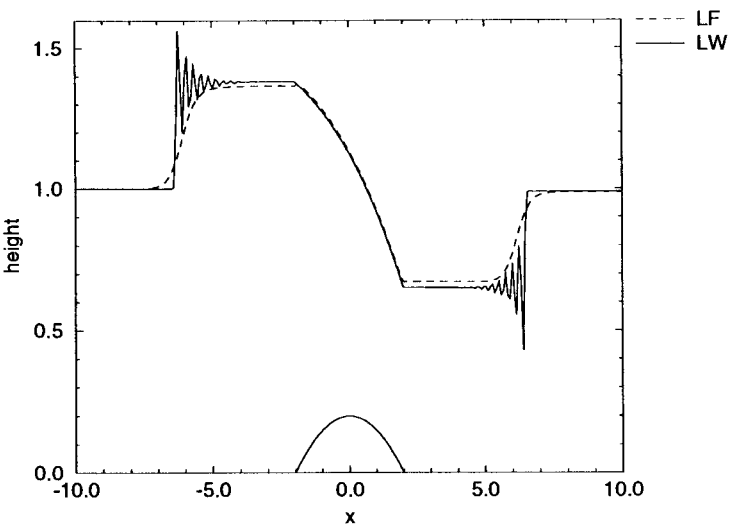


Figure 1. Heights of a one-dimensional shallow water flow calculated by LF and LW schemes.

 

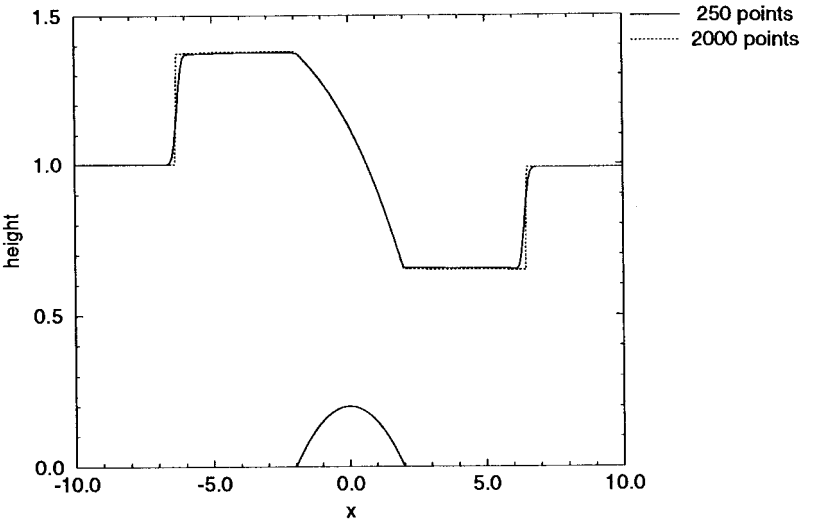


Figure 2. Heights of a one-dimensional shallow water flow calculated by the composite LWLF4 scheme with 250 and 2000 points.

The LW scheme is second-order, while LF is only first-order-accurate, which implies that the composite scheme is also only first-order, however, with a smaller coefficient of the leading error term.

For more details of composite schemes, examples with two-dimensional gas dynamics Riemann problems and tests with a second-order diffusive WENO scheme instead of LF, see Reference [1].

## 3. TWO-DIMENSIONAL SHALLOW WATER EQUATIONS

The shallow water system in two dimensions is described by the fluid layer thickness $h(t, x, y)$, $x$ and $y$ components of layer velocity $u(t, x, y)$, $v(t, x, y)$. The shallow water equations are derived from the three-dimensional Euler equations by vertical averaging using the hydrostatic pressure assumption. For the numerical solution, the authors use the conservative form of the shallow water equations for the conserved momenta $hu$ and $hv$ in the form

$$\begin{aligned} &h_t + (hu)_x + (hv)_y = 0, \\ &(hu)_t + \left(hu^2 + \frac{1}{2}gh^2\right)_x + (huv)_y = 0, \\ &(hv)_t + (huv)_x + \left(hv^2 + \frac{1}{2}gh^2\right)_y = 0, \end{aligned} \tag{4}$$

where $g$ is the gravitation constant. The $x$ and $y$ flux Jacobian matrices of the system are

$$\mathbf{A} = \begin{pmatrix} 0 & 1 & 0 \\ gh - u^2 & 2u & 0 \\ -uv & v & u \end{pmatrix}, \qquad \mathbf{B} = \begin{pmatrix} 0 & 0 & 1 \\ -uv & v & u \\ gh - v^2 & 0 & 2v \end{pmatrix},$$

with eigenvalues $\{u, u \pm \sqrt{gh}\}$ and $\{v, v \pm \sqrt{gh}\}$ respectively.

 

At the inflow boundary, the authors use fixed boundary conditions fixing the values of $h$, $u$, $v$ on the boundary to a given value. At the free boundaries, they use free boundary conditions, setting $h_n = 0$, $u_n = 0$, $v_n = 0$, where the subscript n denotes the derivative normal to the boundary. At the wall boundaries, they use free-slip boundary conditions, setting $h_n = 0$ and the velocity component normal to the boundary is set to zero.

## 4. FINITE DIFFERENCE SCHEMES ON UNIFORM RECTANGULAR MESH

A uniform rectangular mesh is given by the points $(x_i, y_j)$ with constant grid steps $\Delta x = x_{i+1} - x_i$, $\Delta y = y_{j+1} - y_j$. The dual mesh is given by the points $(x_{i+1/2}, y_{j+1/2}) = (x_i + \Delta x/2,\ y_j + \Delta y/2)$. The basic idea of the new version of two-dimensional LF, which is derived in [1], is based on the observation of Boukadida and LeRoux [15], that in order to implement a two-dimensional Godunov method to get cell averages on the dual grid from the averages on the primary grid, one needs only solve one-dimensional Riemann problems on the edges of the dual grid. The first half-step of the new LF is, for the system of conservation laws in two dimensions

$$U_t = f_x(U) + g_y(U), \tag{5}$$

given by

$$U^{n+1/2}_{i+1/2,j+1/2} = \frac{1}{4}[U^n_{i,j} + U^n_{i+1,j} + U^n_{i,j+1} + U^n_{i+1,j+1}] + \frac{\Delta t}{2\Delta x}[F_{i+1,j+1/2} - F_{i,j+1/2}] + \frac{\Delta t}{2\Delta y}[G_{i+1/2,j+1} - G_{i+1/2,j}], \tag{6}$$

where the fluxes $F$, $G$ are evaluated at the LF approximate solution of the one-dimensional Riemann problems at time level $n + 1/4$, giving

$$F_{i+1,j+1/2} = f\left(\frac{1}{2}[U^n_{i+1,j+1} + U^n_{i+1,j}] + \frac{\Delta t}{4\Delta y}[g(U^n_{i+1,j+1}) - g(U^n_{i+1,j})]\right), \tag{7}$$

and

$$G_{i+1/2,j+1} = g\left(\frac{1}{2}[U^n_{i+1,j+1} + U^n_{i,j+1}] + \frac{\Delta t}{4\Delta x}[f(U^n_{i+1,j+1}) - f(U^n_{i,j+1})]\right). \tag{8}$$

The second half-step of the LF scheme going from the dual to the primary mesh is given by the same formulae shifted by 1/2 in the indices $i$ and $j$.

The corresponding second-order-accurate predictor–corrector scheme, which is called the corrected Lax–Friedrichs (CF), is then

$$U^{n+1}_{i,j} = U^n_{i,j} + \frac{\Delta t}{2\Delta x}[f(U^{n+1/2}_{i+1/2,j+1/2}) + f(U^{n+1/2}_{i+1/2,j-1/2}) - f(U^{n+1/2}_{i-1/2,j+1/2}) - f(U^{n+1/2}_{i-1/2,j-1/2})] + \frac{\Delta t}{2\Delta y}[g(U^{n+1/2}_{i+1/2,j+1/2}) + g(U^{n+1/2}_{i-1/2,j+1/2}) - g(U^{n+1/2}_{i+1/2,j-1/2}) - g(U^{n+1/2}_{i-1/2,j-1/2})],$$

where the predictor half-step is defined by the LF half-step (6). One could think about averaging $U^{n+1/2}$ before applying $f$ or $g$. The authors have tried this idea; however, it does not work well for the shock focusing example from Section 6.2.

The composite schemes are constructed in the same way as in one dimension (3) and are denoted by CFLF$k$. For more details see [1], where the authors have shown that both the LF

 

and CF schemes are optimally stable for the scalar advection equation (5) with $f = aU$, $g = bU$, i.e. their stability condition is $\max(|a\Delta t/\Delta x|, |b\Delta t/\Delta y|) \leq 1$, which is also the stability condition of the composite schemes in that case. No stability analysis is available for systems, but the computations indicate that the composite schemes for shallow water are stable with the condition

$$\max(|u \pm \sqrt{gh}|\Delta t/\Delta x, |v \pm \sqrt{gh}|\Delta t/\Delta y) \leq 1.$$

The time interval $\Delta t$ is adaptively determined from this stability condition after each time step.

In [1], the authors have also experimented with a second-order diffusive WENO [16] scheme replacing the LF step in the composite schemes. They do not use the eigenvector decomposition as in [16] and apply the WENO procedure directly to the conserved variables. They call such a scheme component-wise WENO (CW) and the composite is then CFCW*k*. One numerical test of this composite is given later.

## 5. TRAPEZOIDAL MESH

For the supercritical channel flow problems described in Section 6.3, the shallow water equations on a mesh with trapezoidal cells needs to be solved. Here, the LF and CF finite difference schemes are developed on trapezoidal meshes.

Both schemes use the standard device of approximating $f_x + g_y$ in a convex polygonal cell with area $A$ by

$$f_x + g_y \equiv \frac{1}{A} \iint (f_x + g_y)\, \mathrm{d}x\, \mathrm{d}y \equiv \frac{1}{A} \oint -f\, \mathrm{d}y + g\, \mathrm{d}x, \tag{9}$$

with the line integral taken counter-clockwise. The integrals of $f$ and $g$ along the edges are then approximated by some form of midpoint or trapezoidal rule.

### 5.1. Mesh

The solution region is a trapezoid defined by four corners $[(x_a, y_a), (x_b, y_b), (x_a, y_c), (x_b, y_d)]$. The grid indices $(i, j)$ correspond to $(x, y)$ co-ordinates. The grid has $(n_i, n_j)$ points in $(x, y)$ directions. The mesh is uniform in the $x$ co-ordinate.

$$\Delta x = \frac{x_b - x_a}{n_i - 1}, \qquad x_i = x_a + (i-1)\Delta x.$$

The trapezoidal mesh is constructed so that the grid intervals in $y$ depend only on the $x$ index $i$, i.e. the $y$ grid step on each grid line parallel to the $y$ co-ordinate axis is constant.

$$\Delta y_i = y_{i,j+1} - y_{i,j} = \Delta y_1 + (i-1)\frac{\Delta y_{n_i} - \Delta y_1}{n_i - 1},$$

where the first and last grid steps are given by

$$\Delta y_1 = \frac{y_c - y_a}{n_{j-1}}, \qquad \Delta y_{n_i} = \frac{y_d - y_b}{n_j - 1}.$$

The $y$ co-ordinates of the node $(i, j)$ are

$$y_{i,j} = y_a + (i-1)\frac{y_b - y_a}{n_i - 1} + (j-1)\Delta y_i.$$

 

The $y$ co-ordinates of the dual staggered grid are

$$y_{i+1/2,j+1/2} = \frac{1}{4}(y_{i,j} + y_{i+1,j} + y_{i+1,j+1} + y_{i,j+1}).$$

The area of the cell $(i+1/2, j+1/2)$, i.e. of the trapezoid with corners at nodes $[(i,j), (i+1,j), (i+1,j+1), (i,j+1)]$ is

$$S_i = \frac{\Delta y_i + \Delta y_{i+1}}{2} \Delta x.$$

The area of the trapezoid with corners $[(i,j), (i+1/2,j), (i+1/2,j+1/2), (i,j+1/2)]$ is

$$s_i = \frac{3\Delta y_i + \Delta y_{i+1}}{16} \Delta x$$

and the area of the trapezoid with corners $[(i+1/2,j), (i+1,j), (i+1,j+1/2), (i+1/2,j+1/2)]$ is

$$s_{i+1/2} = \frac{\Delta y_i + 3\Delta y_{i+1}}{16} \Delta x.$$

### 5.2. LF predictor

A part of the primary grid that is used in the construction of the LF predictor scheme is shown in Figure 3.

The LF predictor operates from the node values on the original grid at the time level $n$ to the dual staggered grid at the time level $n+1/2$, using the staggered Godunov idea of [15] and also (9). For the present special trapezoids, the difference equations are

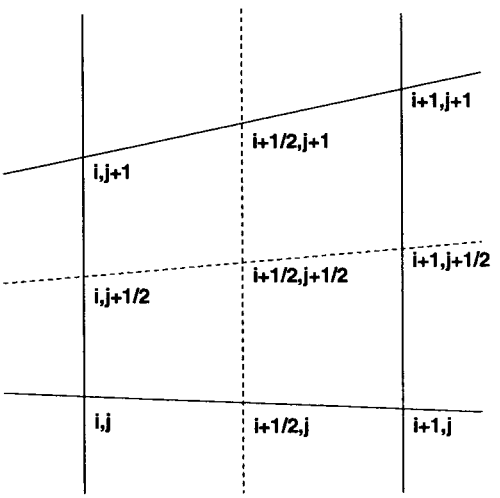


Figure 3. A part of the primary grid used in the LF predictor.

 

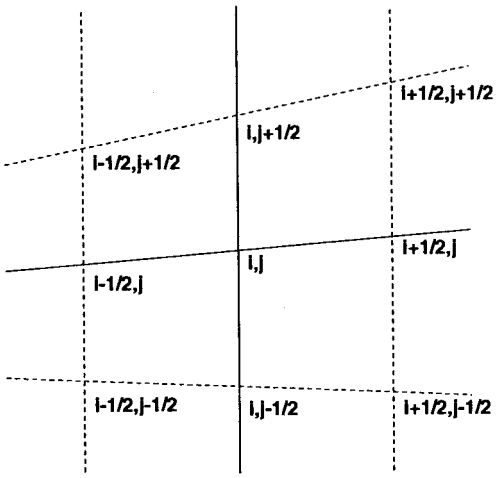


Figure 4. A part of dual grid used in CF corrector.

$$
\begin{aligned}
S_i U_{i+1/2,j+1/2}^{n+1/2} &= s_i U_{i,j}^n + s_{i+1/2} U_{i+1,j}^n + s_{i+1/2} U_{i+1,j+1}^n + s_i U_{i,j+1}^n \\
&- \frac{\Delta t}{2}\left[ - F_{i+1/2,j}(y_{i+1,j} - y_{i,j}) - F_{i+1,j+1/2}(y_{i+1,j+1} - y_{i+1,j}) \right. \\
&\left. + F_{i+1/2,j+1}(y_{i+1,j+1} - y_{i,j+1}) + F_{i,j+1/2}(y_{i,j+1} - y_{i,j}) \right] \\
&+ \frac{\Delta t \Delta x}{2}\left[ G_{i+1/2,j+1} - G_{i+1/2,j} \right],
\end{aligned} \tag{10}
$$

where the fluxes $F$ and $G$ are given by

$$F_{kl} = f(U_{kl}^{n+1/4}), \qquad G_{kl} = g(U_{kl}^{n+1/4}),$$

with $U^{n+1/4}$ denoting the approximate solution of an appropriate one-dimensional Riemann problem. For the horizontally oriented edges, this is a Riemann problem in a rotated co-ordinate system, and the LF approximation is

$$
\begin{aligned}
U_{i+1/2,j}^{n+1/4} &= \frac{1}{2}(U_{i,j}^n + U_{i+1,j}^n) \\
&+ \frac{\Delta t}{4} \frac{(f(U_{i+1,j}^n) - f(U_{i,j}^n))\Delta x + (g(U_{i+1,j}^n) - g(U_{i,j}^n))(y_{i+1,j} - y_{i,j})}{\Delta x^2 + (y_{i+1,j} - y_{i,j})^2},
\end{aligned}
$$

while for the vertical edges, the LF approximation is the same as for a rectangular grid, namely

$$U_{i,j+1/2}^{n+1/4} = \frac{1}{2}(U_{i,j+1}^n + U_{i,j}^n) + \frac{\Delta t}{4} \frac{g(U_{i,j+1}^n) - g(U_{i,j}^n)}{y_{i,j+1} - y_{i,j}}.$$

### *5.3. LF corrector*

The LF corrector is the same as the LF predictor but with the grid shifted by (1/2, 1/2), thereby interchanging the original and dual grids. For completeness, the authors also present the formulae for the LF corrector. For the grid see Figure 4. There is a need here for the area of the cell with center at the node $(i, j)$

 

$$S_{i-1/2} = 2(s_{i-1/2} + s_i)$$

(cell is denoted by its lower left corner). The LF corrector is then

$$\begin{aligned} S_{i-1/2} U_{i,j}^{n+1} &= s_{i-1/2} U_{i-1/2,j-1/2}^{n+1/2} + s_i U_{i+1/2,j-1/2}^{n+1/2} + s_i U_{i+1/2,j+1/2}^{n+1/2} + s_{i-1/2} U_{i-1/2,j+1/2}^{n+1/2} \\ &- \frac{\Delta t}{2} [ - F_{i,j-1/2}(y_{i+1/2,j-1/2} - y_{i-1/2,j-1/2}) - F_{i+1/2,j}(y_{i+1/2,j+1/2} - y_{i+1/2,j-1/2}) \\ &+ F_{i,j+1/2}(y_{i+1/2,j+1/2} - y_{i-1/2,j+1/2}) + F_{i-1/2,j}(y_{i-1/2,j+1/2} - y_{i-1/2,j-1/2})] \\ &+ \frac{\Delta t \Delta x}{2} [G_{i,j+1/2} - G_{i,j-1/2}], \end{aligned}$$

where the fluxes $F$ and $G$ are given by

$$F_{kl} = f(U_{kl}^{n+3/4}), \qquad G_{kl} = g(U_{kl}^{n+3/4}),$$

with

$$\begin{aligned} U_{i,j+1/2}^{n+3/4} &= \frac{1}{2}(U_{i-1/2,j+1/2}^{n+1/2} + U_{i+1/2,j+1/2}^{n+1/2}) \\ &\quad + \frac{\Delta t}{4}\left[\frac{(f(U_{i+1/2,j+1/2}^{n+1/2}) - f(U_{i-1/2,j+1/2}^{n+1/2}))\Delta x}{\Delta x^2 + (y_{i+1/2,j+1/2} - y_{i-1/2,j+1/2})^2}\right. \\ &\quad \left. + \frac{(g(U_{i+1/2,j+1/2}^{n+1/2}) - g(U_{i-1/2,j+1/2}^{n+1/2}))(y_{i+1/2,j+1/2} - y_{i-1/2,j+1/2})}{\Delta x^2 + (y_{i+1/2,j+1/2} - y_{i-1/2,j+1/2})^2}\right], \\ U_{i+1/2,j}^{n+3/4} &= \frac{1}{2}(U_{i+1/2,j+1/2}^{n+1/2} + U_{i+1/2,j-1/2}^{n+1/2}) + \frac{\Delta t}{4}\frac{g(U_{i+1/2,j+1/2}^{n+1/2}) - g(U_{i+1/2,j-1/2}^{n+1/2})}{y_{i+1/2,j+1/2} - y_{i+1/2,j-1/2}}. \end{aligned}$$

### 5.4. CF corrector

A part of the dual grid that is used in the construction of the CF corrector scheme is shown in Figure 4.

The CF predictor is the same as the LF predictor (10). The CF corrector operates from the node values on the dual staggered grid at the time level $n + 1/2$ to the original grid at the time level $n + 1$ and is given by

$$U_{i,j}^{n+1} \equiv U_{i,j}^{n} + \frac{\Delta t}{A} \iint (f_x + g_y)\, \mathrm{d}x\, \mathrm{d}y.$$

Using (9), in this case the equations are

$$\begin{aligned} U_{i,j}^{n+1} = U_{i,j}^{n} &+ \frac{\Delta t}{2S_{i-1/2}} [(f(U_{i+1/2,j-1/2}^{n+1/2}) - f(U_{i-1/2,j+1/2}^{n+1/2}))(y_{i+1/2,j+1/2} - y_{i-1/2,j-1/2}) \\ &+ (f(U_{i+1/2,j+1/2}^{n+1/2}) - f(U_{i-1/2,j-1/2}^{n+1/2}))(y_{i-1/2,j+1/2} - y_{i+1/2,j-1/2}) \\ &+ \Delta x(g(U_{i+1/2,j+1/2}^{n+1/2}) + g(U_{i-1/2,j+1/2}^{n+1/2}) - g(U_{i+1/2,j-1/2}^{n+1/2}) - g(U_{i-1/2,j-1/2}^{n+1/2}))]. \end{aligned}$$

This CF scheme appears to be second-order-accurate on smooth grids, like the grids used in Section 6.3. However, it is only first-order-accurate on the rough grids. The accuracy checking has been done by a numerical convergence test with a smooth solution.

The composite schemes on the trapezoidal mesh are constructed from the CF and LF schemes in the same way as in previous cases.

 

## 6. NUMERICAL RESULTS

This section presents several test examples showing how the composite schemes work for the two-dimensional shallow water equations.

### 6.1. Circular dam break problem

This problem was first solved in [2] then also in [12]. The solution area is a square (0, 50 m) × (0, 50 m). In the center of the square is a cylindrical dam with radius 11 m. The initial water level is 10 m inside the dam and 1 m outside the dam and water is initially at rest. Suddenly, the cylindrical wall forming the dam disappears and time evolution of water movement is calculated. The contour plot of water height at time 0.69 s is shown in Figure 5. For a better insight, the authors also present the surface plot in Figure 6. Calculation is done on a grid of 50 × 50 cells as in [2] by the CFLF4 method. The plots show that the circular symmetry is preserved very well. The results agree with [2,12].

### 6.2. Shock focusing problem

The shock focusing problem originates in [17] and has been solved also in [9]. The square domain $(-1.5, 1.5) \times (-1.5, 1.5)$ has again in the center a circular wall of radius 0.35. The initial height is 0.1 inside the wall and 1 outside. Initially the system is at rest. After removing the wall, the circular shock moves inwards, passes through the singularity and then the circular shock expands outwards. The expanding shock at time $t = 1$ is plotted in Figure 7 as a contour

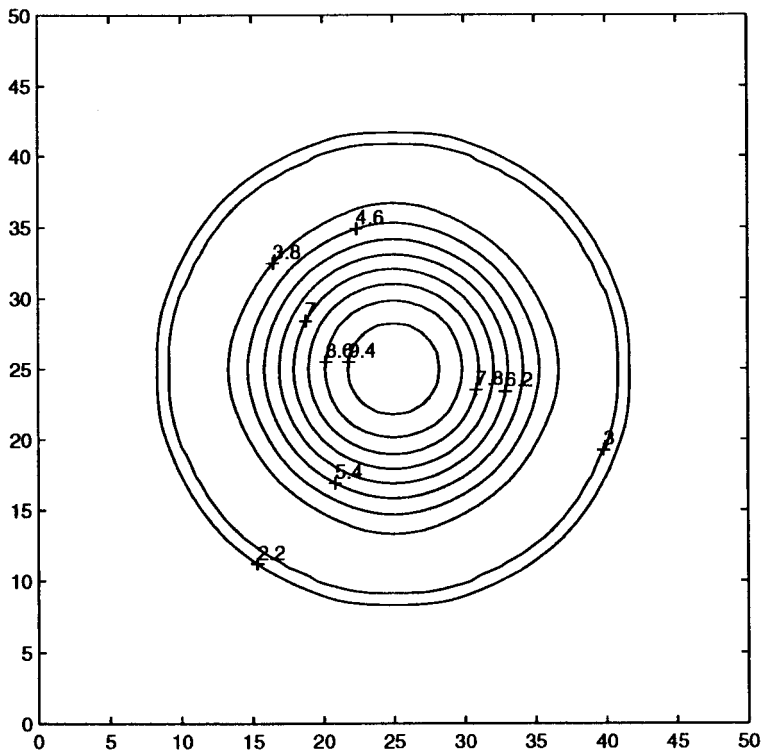


Figure 5. Contour plot of water height for the circular dam break problem.

 

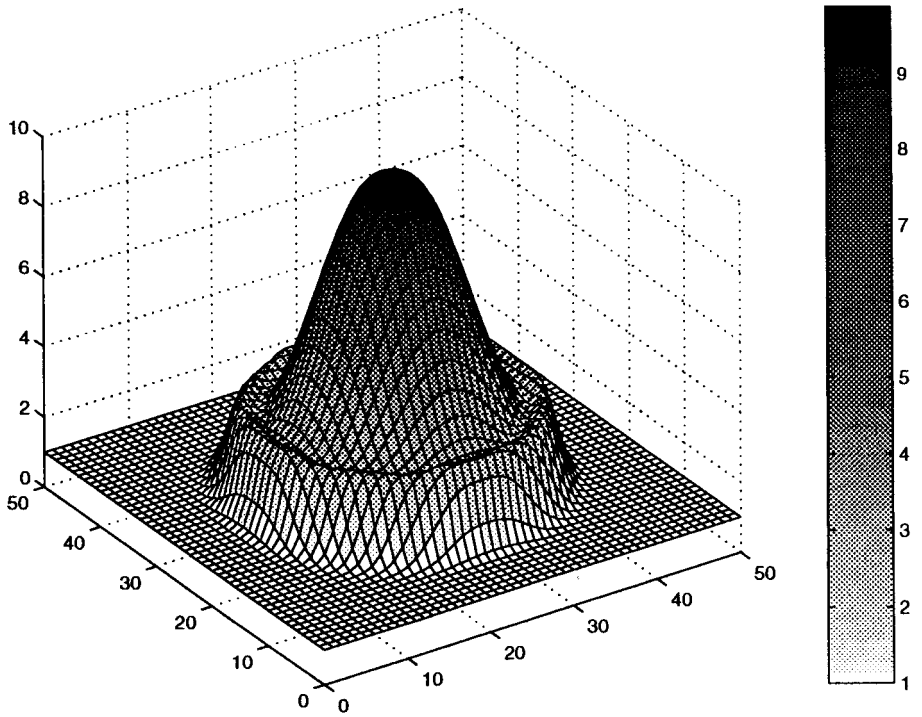


Figure 6. Surface plot of water height for the circular dam break problem.

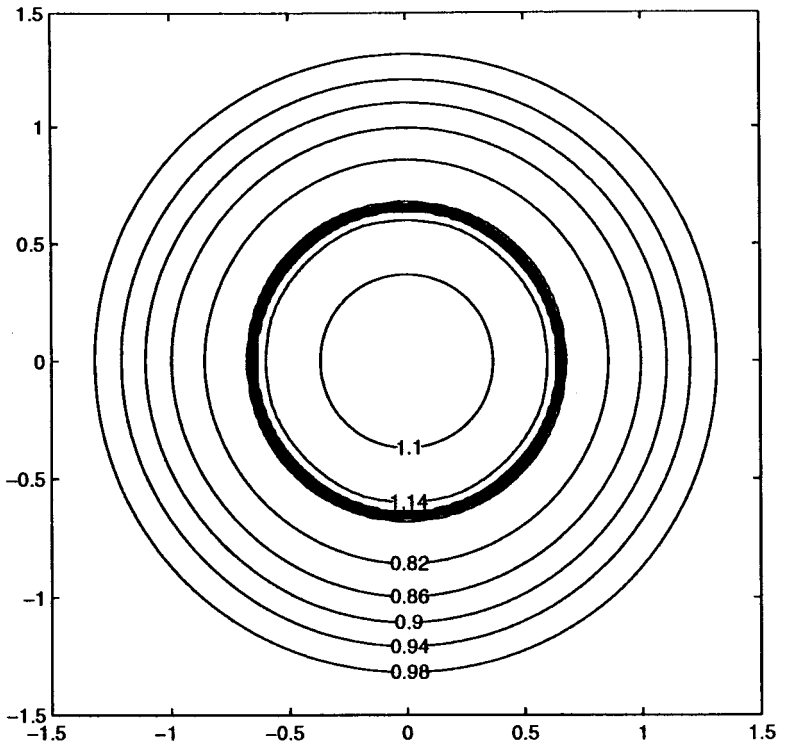


Figure 7. Contour plot of height for the shock focusing problem.

 

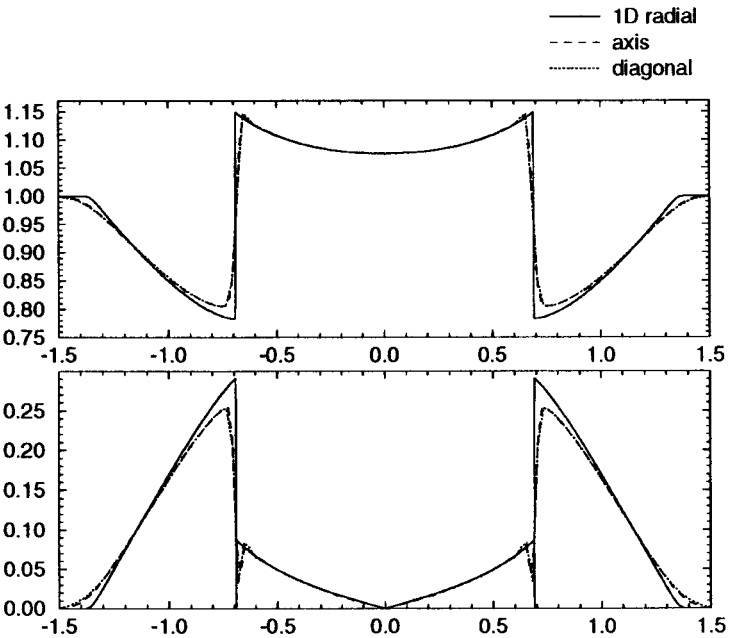


Figure 8. Axis and diagonal profile of height and velocity for the shock focusing problem by CFLF2 scheme. One-dimensional radial symmetric solution is a good approximation of exact solution.

plot. In this calculation, the authors use dimensionless $g = 1$. They use the mesh with $160 \times 160$ points as in [9]. Again circular symmetry is preserved very well.

For comparison, they have also computed the solution of the one-dimensional circularly symmetric shallow water equations

$$H_t + M_r = 0,$$
$$M_t + \left(\frac{M^2}{H} + \frac{1}{2} g \frac{H^2}{r}\right)_r - \frac{1}{2} g \frac{H^2}{r^2} = 0,$$

where $H = hr$ and a conserved momentum $M$ is given by $M = Hu$, by the LWLF4 method on $(0, 1.5)$ with 5000 points. This solution is a good approximation of the exact solution. In Figure 8, the authors compare $x$ and diagonal strips of the two-dimensional CFLF2 solution with the one-dimensional radial symmetric solution. Both height (upper plot) and velocity are plotted. Even for this hard problem, shocks are resolved quite well, $x$ and diagonal strips are almost same. Recall that CFLF2 is only a first-order method.

The authors have also tried the second-order CFCW2 composite scheme. The comparison of $x$ and diagonal strips for height and velocity with the one-dimensional radial solution is in Figure 9. The solution is resolved a bit better in continuum areas. Symmetry is preserved again very well. Note that in [9], two second-order methods had difficulties with velocity differences of $x$ and diagonal strips around the origin.

### *6.3. Supercritical channel flows*

These supercritical (Froude number $F_r = u/\sqrt{gh} > 1$) flow test cases include flows through the channel with wall constrictions. Their solution is a steady state flow with hydraulic and negative jumps. Wall constriction is given by the angle $\alpha$.

 

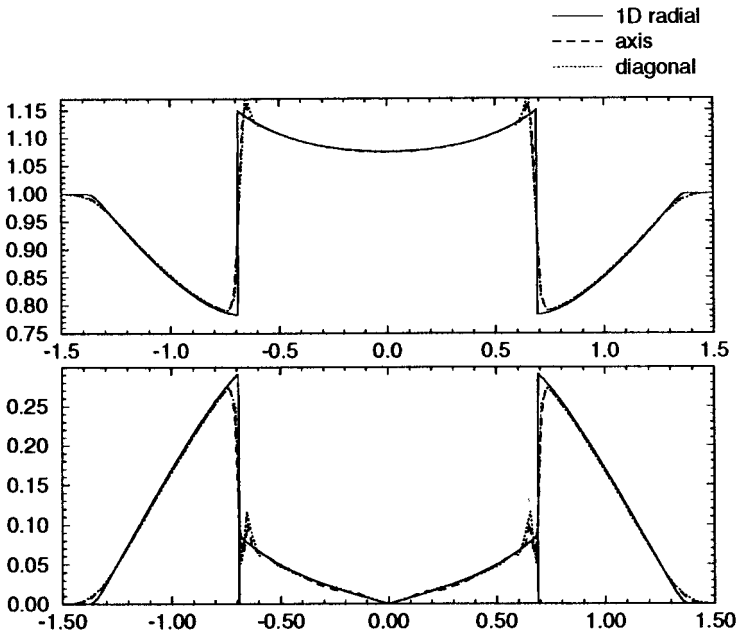


Figure 9. Axis and diagonal profile of height and velocity for the shock focusing problem by CFCW2 scheme. The one-dimensional radially symmetric solution is a good approximation of the exact solution.

*6.3.1. Oblique hydraulic jump*. The first problem is with the wall constriction given by the angle $\alpha = 8.95°$. The initial and inflow conditions are the height $h_0 = 1$ m and velocity $u_0 = 8.57$ m s$^{-1}$. The geometry of the problem with the $41 \times 31$ mesh is given in Figure 10. At the

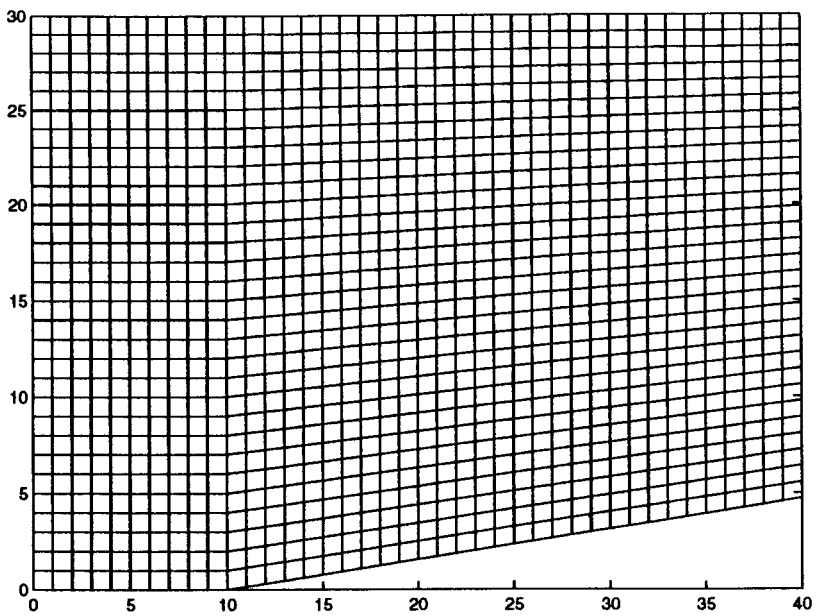


Figure 10. Geometry and mesh for the oblique hydraulic jump problem with $\alpha = 8.95°$.

 

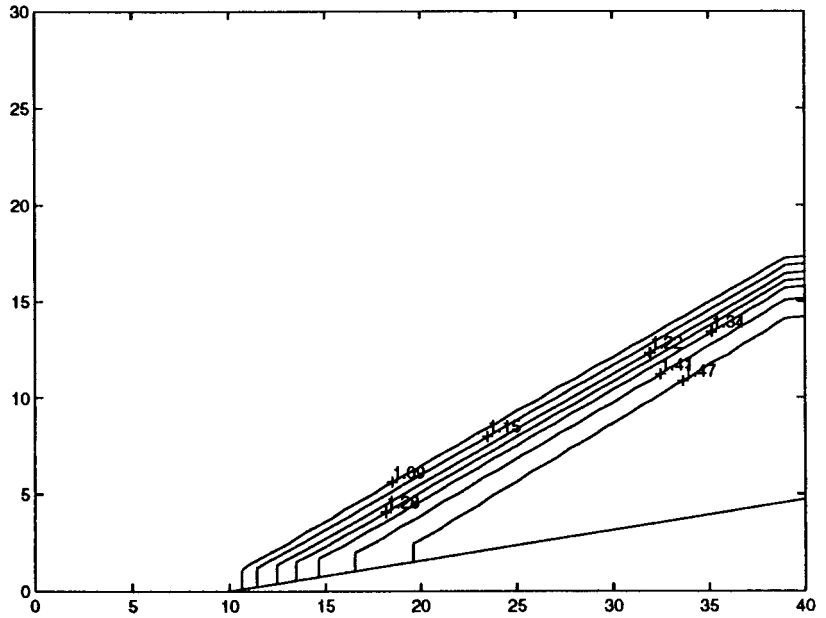


Figure 11. Contour plot of the oblique hydraulic jump problem with $\alpha = 8.95°$.

inflow, left-hand-side, the authors have used inflow, fixed boundary conditions, at the upper and right outflow sides, they have used free boundary conditions and at the lower wall side, slip (free height and zero normal velocity) boundary conditions. The contour plot of the steady

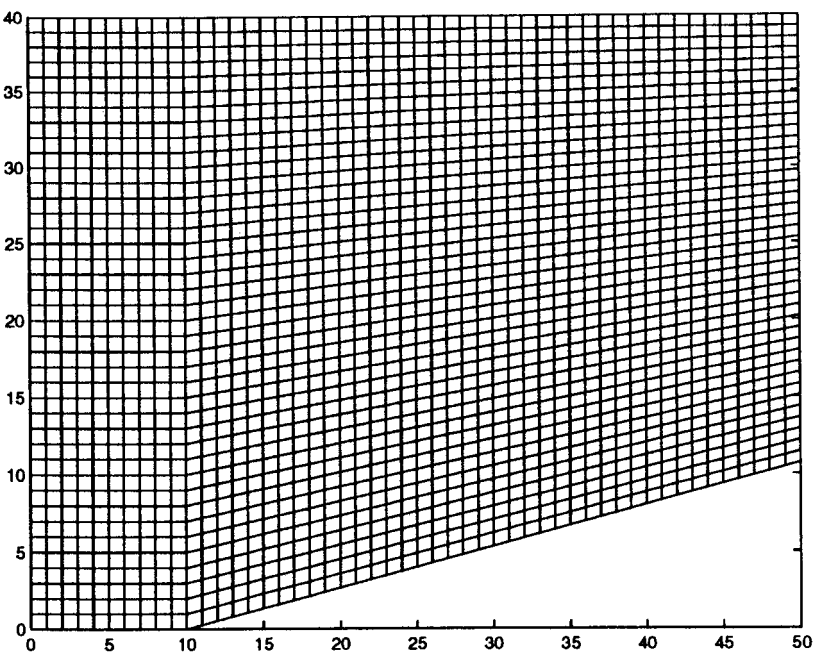


Figure 12. Geometry and mesh for the oblique hydraulic jump problem with $\alpha = 15°$.

 

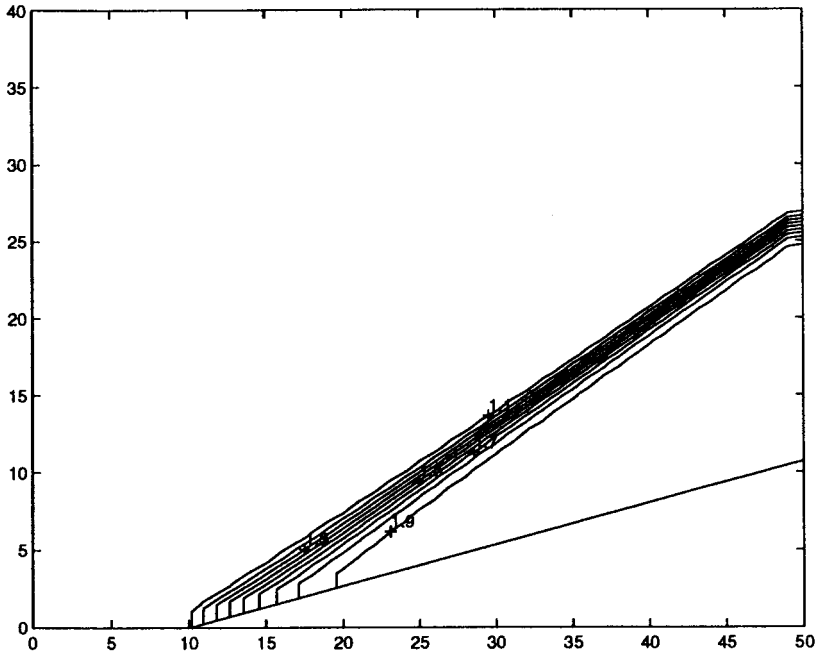


Figure 13. Contour plot of the oblique hydraulic jump problem with $\alpha = 15°$.

state solution is shown in Figure 11. For this problem, the analytical solution can be computed. The shock angle, $\beta = 29.72°$ from the numerical solution agrees well with the analytical result $\beta = 30°$ [2]. Also, the numerical height and velocity $h_2 = 1.5005$, $|u_2| = 7.9787$, agree well with the analytical prediction $h_2 = 1.5$, $|u_2| = 7.9556$ [2].

The second problem is the wall constriction given by the angle $\alpha = 15°$. The initial and inflow conditions are height $h_0 = 1$ and Froude number $F_r = 3$. The geometry of the problem with the $55 \times 37$ mesh is given in Figure 12. The boundary conditions were the same as in the previous test. The contour plot of the steady state solution is given in Figure 13. The shock angle $\beta = 34.14°$ from the numerical solution agrees well with the analytical result, $\beta = 34.36°$ [6].

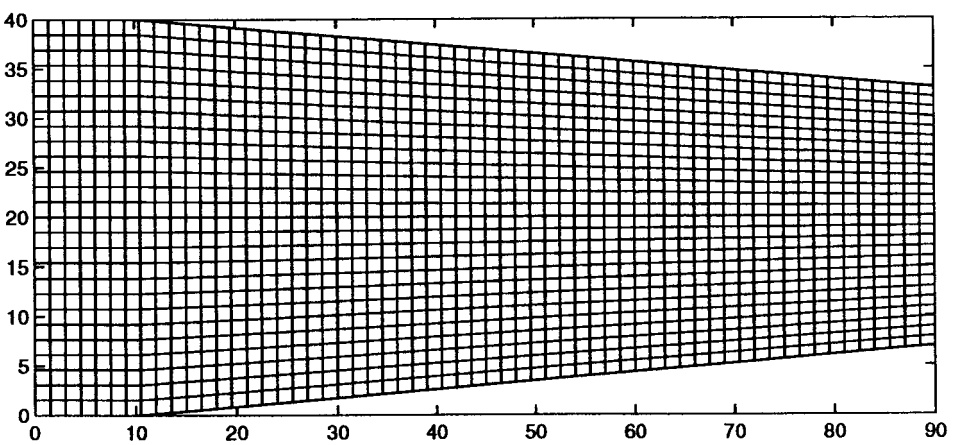


Figure 14. Geometry and mesh for the symmetric channel constriction problem.

 

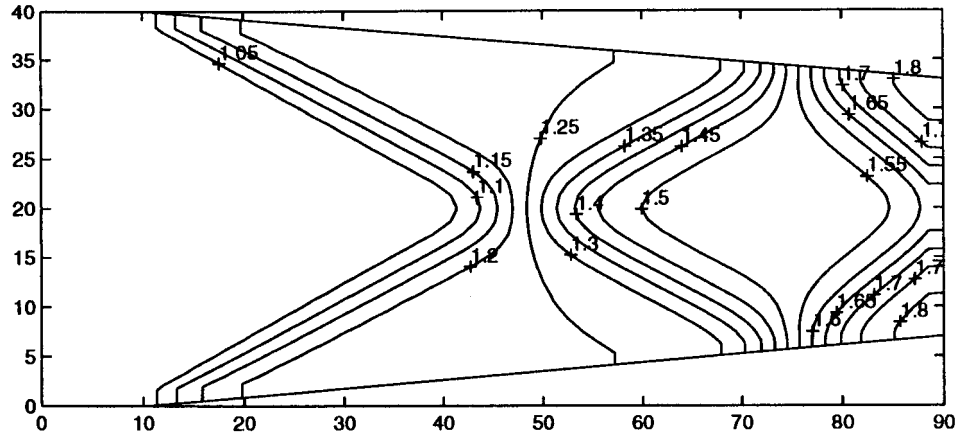


Figure 15. Contour plot for the symmetric channel constriction problem.

*6.3.2. Symmetric channel constriction.* In this example, the channel wall is symmetrically constricted from both sides with angle $\alpha = 5°$. The initial and inflow conditions are the height $h_0 = 1$ and Froude number $F_r = 2.5$. The geometry of the problem with the $61 \times 27$ mesh is given in Figure 14. The contour plot of the steady state solution is in Figure 15 and shows the cross-wave pattern. For more insight, the authors also present the surface plot in Figure 16. In this case, again, they can compare numerical results with analytical ones [6]. Numerical values

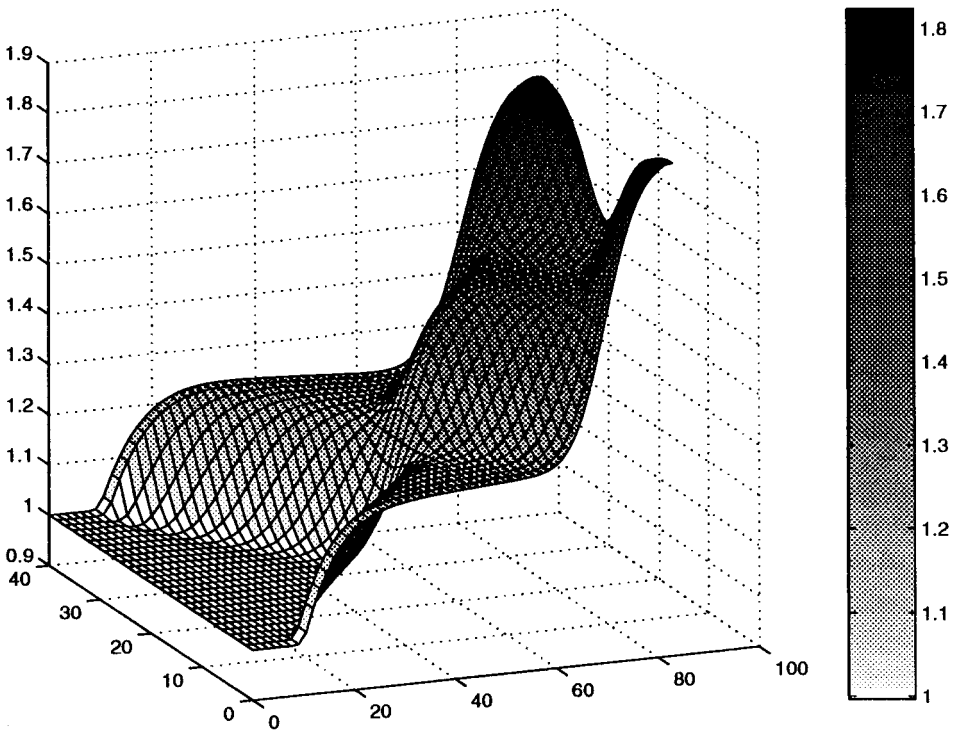


Figure 16. Surface plot for the symmetric channel constriction problem.

 

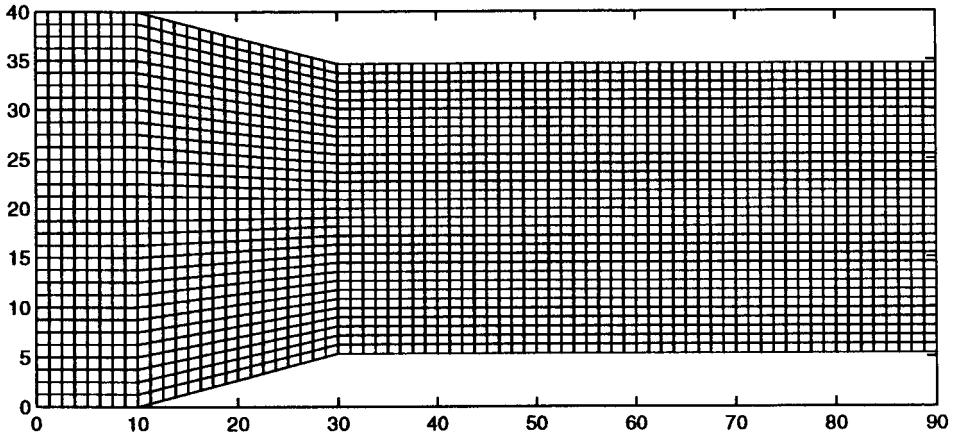


Figure 17. Geometry and mesh for the symmetric channel with variable width problem.

of the heights $h_2 = 1.249$, $h_3 = 1.527$ of the first and second plateau agree well with analytical results $h_2 = 1.254$, $h_3 = 1.55$ [6].

*6.3.3. Symmetric channel with variable width.* In the last example (taken from [6,13]) the channel wall is symmetrically constricted from both sides with angle $\alpha = 15°$ and past the constriction there follows again a straight narrower channel. The geometry of the problem with the $73 \times 33$ mesh is given in Figure 17. The initial and inflow conditions are the height $h_0 = 1$ and Froude number $F_r = 2.5$. The contour plot of the steady state solution is given in Figure 18. For more insight, the authors present the surface plot in Figure 19. The results show again a cross-wave pattern that includes not only hydraulic jumps as in previous examples, but also negative jumps that are caused by the presence of concave corners. On the relatively rough grid, the shocks are again resolved quite nicely with a result similar to that in [13], where they use a grid with a similar number of nodes.

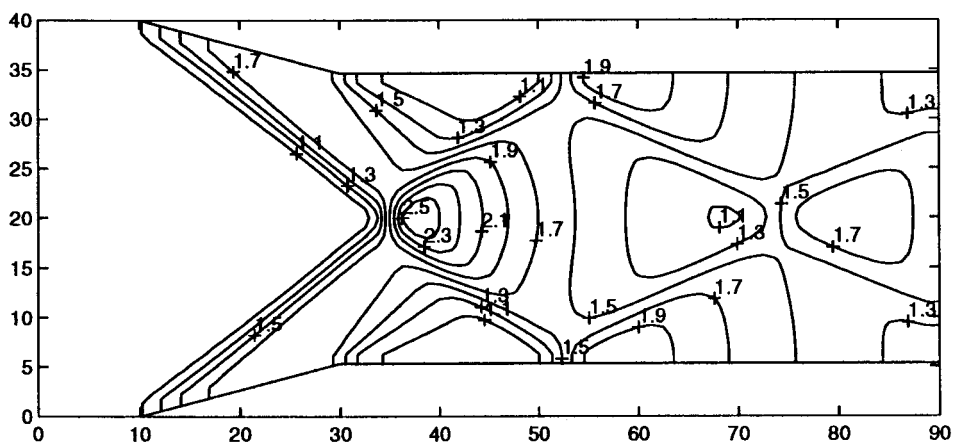


Figure 18. Contour plot for the symmetric channel with variable width problem.

 

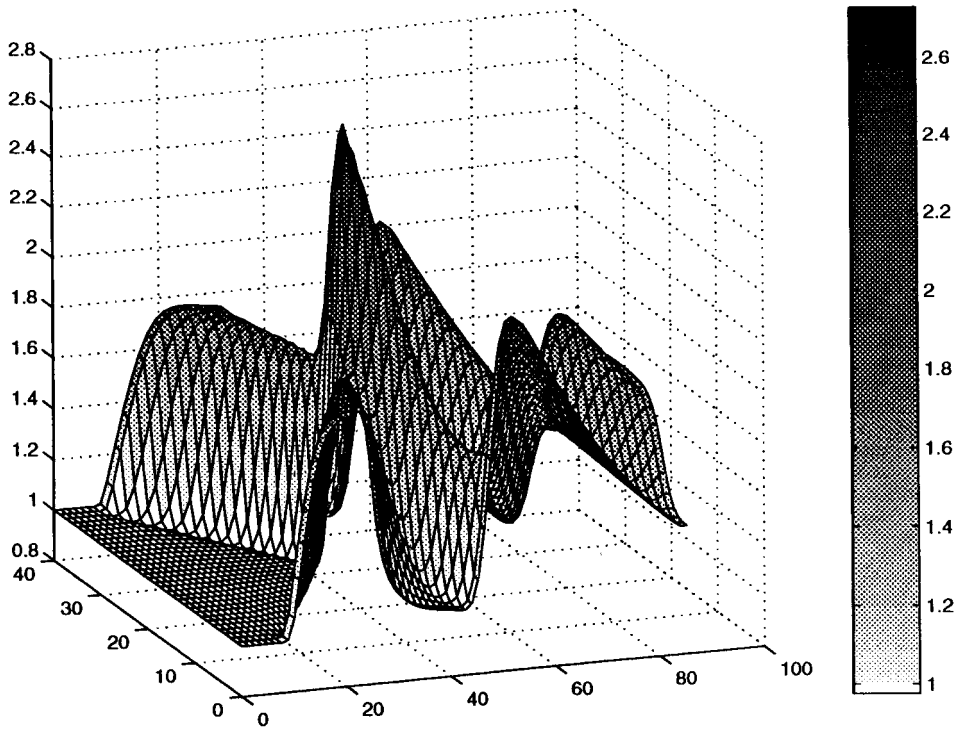


Figure 19. Surface plot for the symmetric channel with variable width problem.

## 7. CONCLUSION

The composite Lax–Wendroff and Lax–Friedrichs schemes have been generalized to trapezoidal meshes and applied to two-dimensional shallow water flows in a constricted channel. This composite and the Lax–Wendroff WENO composite have been applied to the dam breaking problems. The effectiveness and robustness of this approach has been shown on several test examples. Although the authors have not done any speed comparisons with other methods, they believe that these simple schemes result in a rather fast numerical algorithm.

### ACKNOWLEDGMENTS

Both authors were partially supported by the CHAMMP program of the US Department of Energy. R. Liska was supported in part by the National Science Foundation grant CCR-9531828 and Czech Ministry of Education grant Kontakt ME 050 (1997). R. Liska would like to thank the Institute for Geophysics and Planetary Physics of the Los Alamos National Laboratory for hosting his visit at Los Alamos.

### REFERENCES

1. R. Liska and B. Wendroff, 'Composite schemes for conservation laws', *SIAM J. Numer. Anal.*, **35**, 2250–2271 (1998).
2. F. Alcrudo and P. Garcia-Navarro, 'A high resolution Godunov-type scheme in finite volumes for the 2D shallow water equations', *Int. J. Numer. Methods Fluids*, **16**, 489–505 (1993).

 

3. P. Glaister, 'Flux difference splitting for open-channel flows', *Int. J. Numer. Methods Fluids*, **16**, 629–654 (1993).
4. B.T. Nadiga, 'An adaptive discrete velocity model for the shallow water equations', *J. Comp. Phys.*, **121**, 271–280 (1995).
5. B.T. Nadiga, L.G. Margolin and P.K. Smolarkiewicz, 'Semi-Lagrangian shallow water modeling on the CM-5', in A. Ecer, J. Periaux, N. Satofuka and S. Taylor (eds.), *Parallel Computational Fluid Dynamics: Implementations and Results Using Parallel Computers*, *Proceedings of the Parallel CFD'95 Conference*, Pasadena, CA, 26–29 June, 1995, Elsevier, Amsterdam, 1996, pp. 529–536.
6. O.C. Zienkiewicz and P. Ortiz, 'A split-characteristic based finite element model for the shallow water equations', *Int. J. Numer. Methods Fluids*, **20**, 1061–1080 (1995).
7. D. Ambrosi, 'Approximation of shallow water equations by Roe's Riemann solver', *Int. J. Numer. Methods Fluids*, **20**, 157–168 (1995).
8. S.W. Bova and G.F. Carey, 'An entropy variable formulation and applications for the two-dimensional shallow water equations', *Int. J. Numer. Methods Fluids*, **23**, 29–46 (1996).
9. A.T. Morel, M. Fey and J. Maurer, 'Multi-dimensional high-order method of transport for the shallow water equations', in J.A. Desideri, C. Hirsch, P. Le Tallec, M. Pandolfi and J. Periaux (eds.), *Computational Fluid Dynamics '96*, *Proceedings of the Third ECCOMAS Computational Fluid Dynamics Conference*, Paris, 9–18 September 1996, Wiley, New York, 1996, pp. 993–999.
10. P.R.M. Lyra and K. Morgan, 'Adaptive unstructured grid solutions of supercritical shallow water flows', in J.A. Desideri, C. Hirsch, P. LeTallec, M. Pandolfi and J. Periaux (eds.), *Computational Fluid Dynamics '96*, *Proceedings of the Third ECCOMAS Computational Fluid Dynamics Conference*, Paris, 9–18 September 1996, Wiley, New York, 1996, pp. 1012–1018.
11. R.A. Walters and E.J. Barragy, 'Comparison of *H* and *P* finite element approximations of the shallow water equations', *Int. J. Numer. Methods Fluids*, **24**, 61–79 (1997).
12. K. Anastasiou and C.T. Chan, 'Solution of the 2D shallow water equations using the finite volume method on unstructured triangular meshes', *Int. J. Numer. Methods Fluids*, **24**, 1225–1245 (1997).
13. S. Chippada, C.N. Dawson, M.L. Martinez and M.F. Wheeler, 'A Godunov-type finite volume method for the system of shallow water', *Tech. Rep. 96-57*, TICAM, University of Texas, Austin, 1996.
14. D.D. Houghton and A. Kasahara, 'Non-linear shallow fluid flow over an isolated ridge', *Comm. Pure Appl. Math.*, **21**, 1–23 (1968).
15. T. Boukadida and A.-Y. LeRoux, 'A new version of the two-dimensional Lax–Friedrichs scheme', *Math. Comp.*, **63**, 541–553 (1994).
16. Guan-Shan Jiang and Chi-Wang Shu, 'Efficient implementation of weighted eno schemes', *J. Comp. Phys.*, **126**, 202–228 (1996).
17. S.J. Billet, 'A class of upwind methods for conservation laws', *Ph.D. Thesis*, Cranfield University, 1994.

 